J Therm Anal Calorim (2015) 119:1867–1874
DOI 10.1007/s10973-014-4363-5

Solid–liquid interfacial energy of solid succinonitrile in equilibrium with succinonitrile-1,4-diiodobenzene eutectic liquid

Ş. B. Ersoy · Y. Altıntas · S. B. Karadağ · S. Aksöz · K. Keşlioğlu · N. Maraşlı

Received: 11 April 2014 / Accepted: 18 December 2014 / Published online: 28 January 2015

Abstract The grain boundary groove shapes for equilibrated solid SCN in equilibrium with the SCN-0.5 mol% DIB eutectic liquid have been directly observed by using a horizontal linear temperature gradient apparatus. The ratio of thermal conductivity of equilibrated liquid to thermal conductivity of solid SCN has also been determined to be 0.90. From the observed grain boundary groove shapes and measured thermal conductivity ratio, the Gibbs–Thomson coefficient (Γ) of solid SCN has been determined to be $(5.46 \pm 0.55) \times 10^{-8}$ K m. The solid–liquid interfacial energy (σ_{SL}) and the grain boundary energy of solid SCN have also been determined to be $(8.25 \pm 1.24) \times 10^{-3}$ J m^{-2} and $(15.84 \pm 2.53) \times 10^{-3}$ J m^{-2}, respectively.

Ş. B. Ersoy · S. B. Karadağ
Department of Physics, Institute of Science and Technology, Erciyes University, 38039 Kayseri, Turkey

Y. Altıntas
Department of Materials Science and Nanotechnology, Faculty of Engineering and Natural Science, Abdullah Gül University, 38039 Kayseri, Turkey

S. Aksöz
Department of Physics, Faculty of Arts and Sciences, Nevşehir Hacı Bektaş Veli University, 50300 Nevşehir, Turkey

K. Keşlioğlu (✉)
Department of Physics, Faculty of Science, Erciyes University, 38039 Kayseri, Turkey
e-mail: kesli@erciyes.edu.tr

N. Maraşlı
Department of Metallurgical and Materials Engineering, Faculty of Chemical and Metallurgical Engineering, Yıldız Technical University, Davutpaşa, 34210 Istanbul, Turkey

Keywords Phase equilibria · Interfaces · Organic compounds

Introduction

The solid–liquid interfacial energy (σ_{SL}) plays a key role in a wide range of metallurgical and materials phenomena from wetting [1] and sintering to phase transformations and coarsening [2]. For example, any meaningful comparison between experimentally observed solidification morphology and predictions from theoretical models requires an accurate knowledge of solid–liquid interfacial energy. Thus, a quantitative knowledge of σ_{SL} values is necessary. However, the determination of σ_{SL} is difficult. The earliest direct determinations were derived from droplet undercooling measurements on the supposition that maximum observed undercooling signified homogeneous nucleation. An empirical relationship between the interfacial energy and enthalpy of fusion to estimate the interfacial energy was proposed by Turnbull [3], and it is expressed as

$$\sigma_{SL} = \frac{\tau \Delta H_M}{V_S^{2/3} N_a^{1/3}} \quad (1)$$

where τ is a coefficient, found to be 0.45 for metals (especially, closely packed metals) and 0.34 for nonmetallic systems at about 20 % of undercooling below the melting point [3], ΔH_M is the enthalpy of fusion, V_S is the molar volume of solid phase and N_a is the Avogadro's number. However, the next experiments show that larger values of undercooling, resulting in larger values of σ_{SL}, indicating that such experiments typically underestimate σ_{SL}. Other disadvantages of deriving σ_{SL} from undercooling experiments were discussed by Jones [4] and Eustathopoulos [5].

A technique for the quantification of solid–liquid interfacial energy from the grain boundary groove shape has been established [3–16]. Observation of groove shape in a thermal gradient can be used to determine the interfacial energy from Gibbs–Thomson equation [16]. For the case of a planar grain boundary intersecting a planar solid–liquid interface, Gibbs–Thomson equation can be written as

$$\Gamma = r\,\Delta T_{\mathrm{r}} = \frac{\sigma_{\mathrm{SL}}}{\Delta S_{\mathrm{f}}} \tag{2}$$

where Γ is the Gibbs–Thomson coefficient and r is radius of groove profile as shown in Fig. 1. Thus, the curvature undercooling, ΔT_{r}, is a function of curvature radius, solid–liquid interfacial energy and the entropy of fusion per unit volume. This equation is useful for considering the effect of solid–liquid interfacial energy on solidification and melting as it expresses the effective change in melting point for a curved interface.

Gündüz and Hunt [17] developed an apparatus to observe the equilibrated grain boundary groove shapes in opaque metallic binary systems. The details of apparatus and experimental procedures are given in Ref. [17]. Gündüz and Hunt [17] also developed a finite difference model to calculate the Gibbs–Thomson coefficient. Usually, the points from **b** to **i** were used to obtain more reliable Γ values with Gündüz and Hunt's model as shown in Fig. 1. If the grain boundary groove shape, the temperature gradient in the solid (G_S) and the ratio of thermal conductivity of the equilibrated liquid phase to thermal conductivity of solid phase ($R = K_{\mathrm{L}}/K_{\mathrm{S}}$) are known or measured, the value of the Gibbs–Thomson coefficient (Γ) is then obtained with the Gündüz and Hunt numerical method. Measurements of the solid–liquid interface energy were made in different metallic binary systems [17–19].

Bayender et al. [20, 21] modified the apparatus originally designed by Hunt et al. [22] to directly observe the equilibrated grain boundary groove shape for transparent materials. They applied Gündüz and Hunt's numerical method to determine the Gibbs–Thomson coefficient, the solid–liquid interface energy and the grain boundary energy. Measurements of the solid–liquid interface energies were also made in transparent organic binary systems [20, 21, 23–30].

The binary phase diagram of succinonitrile (SCN)-1,4-diiodobenzene (DIB) was determined by Kant [31] and is shown in Fig. 2. The synthesis and solidification behaviour of monotectic alloy are of potential importance both from fundamental understanding of the development of self-lubricating alloys and for industrial applications [32, 33]. Although, metallic systems, giving monotectic alloys, constitute an interesting area of investigations [34–36], due to high transformation temperature and wide density difference of the components, they are not suitable for detail study. However, low transformation temperature, transparency, wider choice of materials and minimized convection effects are the special features that have prompted a number of research groups [37, 38] to work on organic eutectics, monotectics and molecular complexes. As such, organic systems are used as model systems for detailed investigation of the parameters that control the mechanism of solidification and decide the properties of materials. In addition, these materials are being studied for various physicochemical investigations for their use for nonlinear optical effects and different electronic applications [39–41]. The monotectic alloys have been less studied due to several difficulties associated with the systems show miscibility gap while some of the articles [33, 42, 43] explain various interesting phenomena of monotectic alloys. The main problem arises due

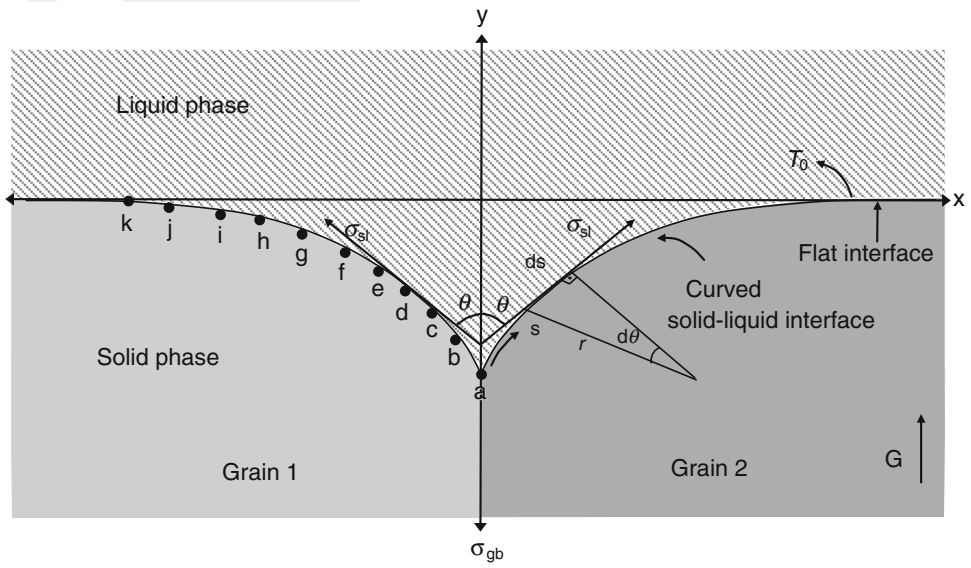

Fig. 1 Schematic illustration of an equilibrated grain boundary groove formed at a solid–liquid interface in a temperature gradient showing the definitions of r, θ and y

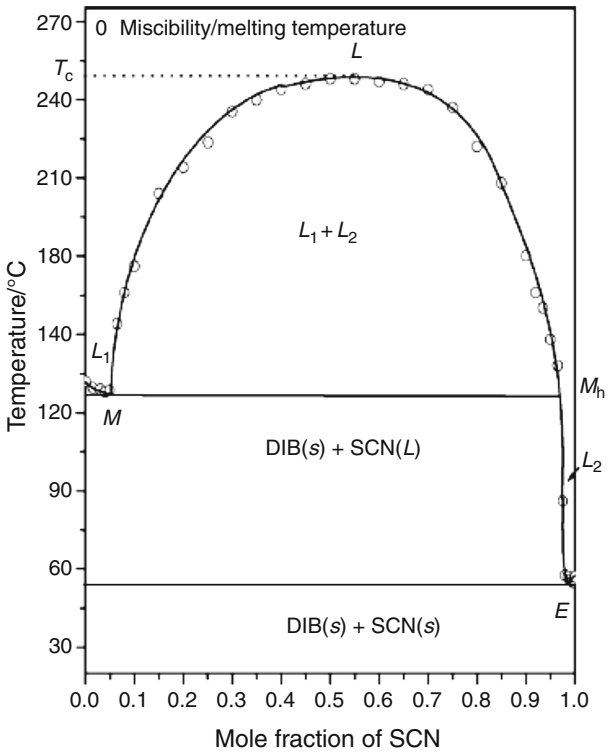

Fig. 2 Phase diagram of succinonitrile-1,4-diiodobenzene system [31]

to a wide freezing range and large density difference between two liquid phases. The role of wetting behaviour, interfacial energy, thermal conductivity and buoyancy in a phase separation process has been the subject of great discussion.

DIB and SCN are used in wide range of industrial applications. For example, the plastic-crystal form of SCN is used for obtaining high ionic conductivity for a large variety of salts dissolved in the highly polar medium. The high diffusivity, plasticity and solvating power of SCN allowed the preparation of a large number of materials with high ionic conductivity. Solid ionic conductors are actively sought for their potential application in electrochemical devices, particularly lithium batteries [44]. DIB is used in a wide range of medicals, industrial applications as well as in human and animal nutrition products such as antiseptics and disinfectants, pharmaceutical intermediates and polarizing films for liquid crystal display (LCD) chemicals. Iodine derivatives are also used as organic building blocks, analytical reagents [45]. DIB is a material of high enthalpy of fusion and simulates the nonmetallic solidification, whereas SCN, a material of low enthalpy of fusion, corresponds the metallic solidification. Therefore, the present SCN–DIB system is very good organic analogue of metal–nonmetal systems like Al–Si and Zn–Bi. In the present paper, the details to determine the Gibbs–Thomson coefficient, solid–liquid interfacial energy and grain boundary energy in the SCN–DIB system are reported.

Materials and methods

Preparation of test materials

The experimental technique requires the preparation of thin slides containing the high-purity test material and the necessary thermocouple assemblies. Accordingly, the preparation of specimens for purified transparent material involved three primary operations: (1) the purification of test materials by distillation, (2) the design and assembly of the thin-slide specimen cell and (3) filling the specimen cell with the purified test materials under the vacuum.

The purities of SCN and DIB were 99 and 98 %, respectively, supplied by Alfa Aesar. SCN and DIB were purified in quantities of approximately 100 cm^3 using a columnar distillation system [26–30]. The distillation was repeated four times, and the distilled material was finally collected in a glass tube, flame-sealed under the vacuum during the distillation.

The experimental technique requires the preparation of rectangular thin slides containing the test material and the necessary thermocouple assemblies. Accordingly, the preparation of specimens for transparent material involves two primary operations: the design and assembly of the thin-slide specimen cell, and filling the specimen cell with the test materials under vacuum.

The specimen cells were fabricated such that the test material was contained between two parallel ground glass plates (50 mm × 24 mm × 0.12 mm). Silicone elastomer glue was used to attach and seal the assembly on three sides with three K-type thermocouples (50 μm in diameter) fixed within the cell, distributed along the length direction with a spacing of 2–3 mm. The distance between the two glass plates was 80–100 μm. Before filling the cell with the test materials, the glue was cured for at least 24 h at room temperature to avoid any reaction between the test materials and the glue.

Test specimens were prepared by the remelting of the SCN-0.4 mol% DIB material under vacuum and then introduced into the prepared glass cells. During this procedure, the material was kept within a specialized filling chamber designed to minimize contamination from ambient air [26–30]. Before the remelting, the chamber atmosphere was evacuated. Within the filling chamber, the open end of the test cell was immersed into the molten SCN-0.4 mol% DIB, and argon gas at a pressure of approximately 15 bars was imposed to force-fill the thin slide. After filling, the slide was permitted to cool until completely solid, and then, the specimen was removed from the chamber. The melting temperature of SCN-0.4 mol% DIB was measured as 328 K from cooling curvature, obtained under vacuum.

The temperature gradient measurement

Bayender et al. [20] utilized a temperature gradient stage to observe the equilibrated grain boundary groove shape in transparent organic materials. In the present work, a similar apparatus was employed to observe the grain boundary groove shapes of solid SCN in equilibrium with SCN-0.5 mol% DIB liquid. The apparatus consists of hot and cold stages. The temperature of the hot stage was controlled within an accuracy of ±0.01 K by a *Eurotherm 2604* type controller. The cold-stage design was similar to that of the hot stage. However, the cooling was achieved using a *PolyScience digital 9102* model heating/refrigerating circulating bath containing an aqueous ethylene glycol solution. The temperature of the circulating baths was kept constant at 278 K with an accuracy of ±0.01 K.

A liquid layer (2 or 3 mm thick) was melted, and the specimen was held in a constant temperature gradient to observe the equilibrated grain boundary groove shape of solid SCN in equilibrium with SCN-0.5 mol% DIB eutectic liquid. The equilibrating time for solid SCN in equilibrium with SCN-0.5 mol% DIB liquid was 3 days. The solid SCN in equilibrium with SCN-0.5 mol% DIB liquid interface was too stable against environmental air fluctuations or turbulence during the equilibrating time. The temperatures in the specimen were measured using three insulated K-type thermocouples with wires (50 μm thick) connected to a data logger via computer. When the solid–liquid interface reached the equilibrium, the temperature difference between two thermocouples (ΔT) was measured, and the positions of the thermocouples and the equilibrated grain boundary groove shapes were then photographed with an *Olympus DP 12* type digital camera placed in conjunction with an *Olympus BHX* type light optical microscope. The distance between two thermocouples (ΔX) was measured by using *Adobe PhotoShop CS3* version software from the photographs of the thermocouple positions.

The temperature gradients ($G = \Delta T/\Delta X$) for each grain boundary groove shapes were determined by using the values of measured ΔT and ΔX. The estimated error in the measurements of temperature gradient (G) is about 5 % [23].

The coordinates of equilibrated grain boundary groove shapes were measured with an optical microscope to an accuracy of ±10 μm. The uncertainty in the measurements of equilibrated grain boundary groove coordinates is 0.1 %.

The ratio of thermal conductivity of equilibrated liquid phase to thermal conductivity of solid phase

The ratio of thermal conductivity of equilibrated liquid phase to the thermal conductivity of solid phase ($R = K_L/K_S$) must be known or measured to evaluate the Gibbs–Thomson coefficient with the present numerical method. The value of R can be obtained during directional growth with a Bridgman-type growth apparatus. During directional growth, the heat flow away from the interface through the solid phase must balance the heat flow from the liquid phase plus the latent heat generated at the interface [46], i.e.

$$VL = K_S G_S - K_L G_L, \tag{3}$$

where V is the growth rate, L is the latent heat, G_S and G_L are the temperature gradients in the solid and liquid phases, respectively. K_S and K_L are the thermal conductivities of solid and liquid phases, respectively. For very low velocities, $VL << K_S G_S - K_L G_L$, so that the thermal conductivity ratio R is given by

$$R = \frac{K_L}{K_S} = \frac{G_S}{G_L} \tag{4}$$

A directional growth apparatus, which was first constructed by McCartney [47], was used to find out the ratio of thermal conductivity of liquid phase to the thermal conductivity of solid phase. A thin-walled graphite tube, which has 6 mm OD (outer diameter), 4 mm ID (inner diameter) and 180 mm total length, was used to minimize convection into the liquid phase. Molten SCN-0.4 mol% DIB was poured into the thin-walled glass tube and then directionally solidified from bottom to top to ensure the filling of the crucible. The specimen was then placed in the directional growth apparatus.

The specimen was heated up to 30 K above the melting temperature of SCN-0.4 mol% DIB. The specimen was then left to reach its thermal equilibrium for at least 2 h. The temperatures in the specimen were measured by insulated K-type thermocouples. In the present work, 1.2 mm OD, 0.8 mm ID alumina tube was used to fix the thermocouples at the centre of sample. At the end of equilibration, the temperature in the specimen was stable to ±0.5 K for short-term period and ±1 K for long-term period. When the specimen temperature was stabilized, directional growth was begun by turning the motor on. The cooling rate was recorded with a data logger via computer. In the present measurement, the growth rate was 8.0×10^{-4} cm s^{-1}. When the solid–liquid interface passed the thermocouple, a change in the slope of the cooling rates for liquid and solid phases was observed. When the thermocouple was reading approximately 20 K below the melting temperature, the growth was stopped by turning the motor off.

The ratio between the thermal conductivity of liquid phase and the thermal conductivity of solid phase can be obtained from the cooling rate of liquid and solid phases. From the cooling rate of the liquid and solid phases, the thermal conductivity ratio can be written as

$$R = \frac{K_L}{K_S} = \frac{G_S}{G_L} = \frac{\left(\frac{dT}{dt}\right)_S}{\left(\frac{dT}{dt}\right)_L} \quad (5)$$

where the values of $\left(dT/dt\right)_S$ and $\left(dT/dt\right)_L$ were directly measured from the curve of temperature versus time shown in Fig. 3. The ratio of thermal conductivity of liquid phase (SCN-0.5 mol% DIB) to thermal conductivity of solid SCN phase was found to be 0.90 from Fig. 3.

Results and discussion

Determination of Gibbs–Thomson coefficient

The Gibbs–Thomson coefficients for solid SCN in equilibrium with the SCN-0.5 mol% DIB eutectic liquid were determined with the present numerical method by using ten observed grain boundary groove shapes, and the results are given in Table 1. Typical grain boundary groove shapes for solid SCN in equilibrium with the SCN-0.5 mol% DIB eutectic liquid are shown in Fig. 4. The experimental error in the determination of Gibbs–Thomson coefficient is given by the sum of errors in measuring the temperature gradient and thermal conductivity. Thus, the total experimental error in the determination of Gibbs–Thomson coefficient was about 10 %. As a consequence, the mean value of Γ for solid SCN in equilibrium with the SCN-0.5 mol% DIB eutectic liquid is found to be $(5.46 \pm 0.55) \times 10^{-8}$ K m from the Table 1.

The entropy of fusion per unit volume

To determine the solid–liquid interfacial free energy, it is also necessary to know the entropy of fusion per unit volume, and it is given by

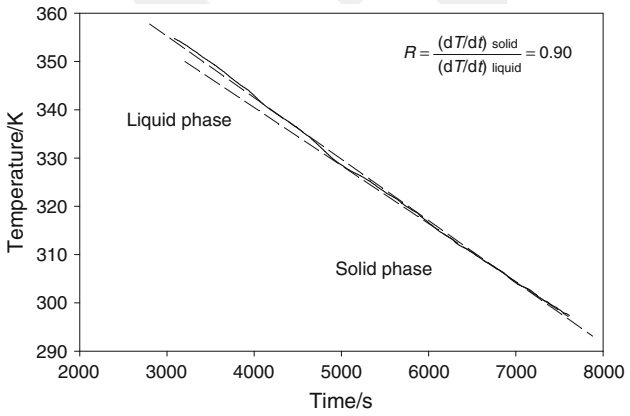

Fig. 3 Cooling curve of SCN-0.4 mol% DIB system

Table 1 Gibbs–Thomson coefficients for solid SCN in equilibrium with SCN-0.5 mol% DIB eutectic liquid

Groove no.	$G_S \times 10^2$/K m^{-1}	Gibbs–Thomson coefficient Γ/K m	
		$\Gamma_{LHS} \times 10^{-8}$	$\Gamma_{RHS} \times 10^{-8}$
1	44.97	5.47	5.21
2	45.87	5.53	5.33
3	51.56	5.35	5.68
4	43.62	5.39	5.30
5	41.45	5.48	5.58
6	45.15	5.55	5.60
7	47.32	5.56	5.24
8	44.43	5.58	5.31
9	43.98	5.36	5.88
10	40.18	5.46	5.39
$\bar{\Gamma} = (5.46 \pm 0.55) \times 10^{-8}$ K m			

The subscripts LHS and RHS refer to left hand side and right hand side of the groove, respectively

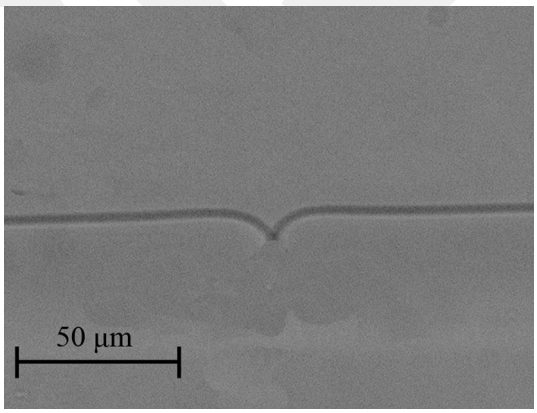

Fig. 4 Typical grain boundary groove shape for solid SCN in equilibrium with the SCN-0.5 mol% DIB eutectic liquid

$$\Delta S_f = \frac{\Delta H_M}{T_M}\frac{1}{V_S} \quad (6)$$

where ΔH_M is the enthalpy change of solid phase at melting temperature, T_M is the melting temperature and V_S is the molar volume of solid phase. The molar volume V_S is expressed as

$$V_S = V_c N_a \frac{1}{n} \quad (7)$$

where V_c is the volume of the unit cell, N_a is the Avogadro's number and n is the number of molecules per unit cell. Some physical properties of solid SCN in equilibrium with SCN-0.5 mol% DIB eutectic liquid are given in Table 2.

Table 2 Some physical properties for solid SCN in equilibrium with SCN-0.5 mol% DIB eutectic liquid

System	SCN–DIB
Solid phase	SCN
Liquid phase	SCN-0.5 mol% DIB
Melting point/T_M	328 K [31]
Molecular volume/V_S	76.50×10^{-6} m^3 mol^{-1} [48]
Enthalpy change/ΔH_M	3,800 J mol^{-1} [31]
Entropy of fusion/ΔS_f	1.51×10^5 J K^{-1} m^{-3}

The entropy of fusion per unit volume (ΔS_f) for solid SCN was calculated to be 1.51×10^5 J K^{-1} m^{-3} by using relevant parameters and is also given in Table 2. The error in the determination of entropy of fusion per unit volume is estimated to be about 5 % [17–19].

The solid–liquid interfacial energy

If the values of the Gibbs–Thomson coefficient and the entropy of fusion per unit volume are measured or known, the solid–liquid interfacial energy can be obtained from Eq. (2). The experimental error in the determination of solid–liquid interfacial energy is the sum of the experimental errors of the Gibbs–Thomson coefficient and entropy of fusion per unit volume. Thus, the total experimental error in the determination of the solid–liquid interfacial energy with the present method was about 15 %. The mean value of the solid–liquid interfacial energy (σ_{SL}) for solid SCN in equilibrium with the SCN–DIB liquid was found to be $(8.25 \pm 1.24) \times 10^{-3}$ J m^{-2}.

As mentioned above, the groove profile method actually measures $\Gamma_{SL} = \sigma_{SL}/\Delta S_f$ so that a value is required for ΔS_f to evaluate σ_{SL}. Substituting Eq. (1) into Eq. (2) gives

$$\Gamma = \tau T_m \left(\frac{V_S}{N_A}\right)^{1/3} = \tau T_m \Omega^{1/3} \tag{8}$$

where Ω is the volume per atom.

Granasy et al. [12] have calculated the values of τ for different orientations of the fcc, hcp, bcc and sc structures. They have found the minimum, maximum and average values of τ for the fcc., hcp, bcc and sc structures. Hoyt et al. [15] have plotted the Turnbull relationship for many fcc and bcc metals via the capillarity fluctuation method (CFM) and also found the values of τ for the fcc and bcc structures. More recently, Jones [49] compared the values of Γ and σ_{SL} measured by groove profile methods with the values of Γ and σ_{SL} measured by other methods and determined the values of τ for metallic binary systems by using the measured values of Γ. He found the values of τ range by 0.13 for Al_3Ni to 1.0 for Al_α. According the values of τ determined by Jones [49], the value of τ changes with the type of materials, and it might be in range from 0.13 to 1.0 for the binary metallic materials. In the present work, the values of τ for some solid SCN phases in equilibrium with different liquids were calculated from Eq. (8) by using the measured values of Γ and V_M, and it is given in Table 3. The average value of τ for solid SCN phase was obtained to be 0.33 from Table 3. It is interesting to observe that the calculated average value of τ for solid SCN is in good agreement with the value of τ calculated from the supercooling experiments performed by Turnbull [3] on nonmetallic materials. It might conclude

Table 3 A comparison of the values of Γ,τ, σ_{SL} and σ_{gb} for solid SCN obtained in the present work with the values of Γ, τ, σ_{SL} and σ_{gb} obtained in previous works for similar eutectic alloys

Solid phase mole pct.	Liquid phase mole pct.	Temperature/K	$V_S \times 10^{-6}$/m^3 mol^{-1}	τ_{expt}	Crystal structure	$\Gamma \times 10^{-8}$/K m	$\sigma_{SL} \times 10^{-3}$/J m^{-2}	$\sigma_{gb} \times 10^{-3}$/J m^{-2}	References
SCN	SCN	331.23	76.50	0.33	bcc	5.43 ± 0.27	7.86 ± 0.79	15.03 ± 1.95	Maraşlı et al. [23]
				0.37		6.2	8.94 ± 0.50	15.95	Schaefer et al. [50]
				0.36		6.1	8.90	–	Jones and Chadwick [7]
SCN	SCN-4 CTB	318.15		0.35		5.56 ± 0.28	8.80 ± 0.88	16.51 ± 2.15	Maraşlı et al. [23]
SCN	SCN-1.8 DBB	325.65		0.33		5.47 ± 0.60	8.12 ± 1.22	15.19 ± 2.58	Böyük and Maraşlı [24]
SCN	SCN-25.6 PY	326.45		0.32		5.21 ± 0.26	9.58 ± 0.96	18.30 ± 2.38	Böyük et al. [25]
SCN	SCN-5.71 DCB	319.15		0.34		5.43 ± 0.27	7.95 ± 0.80	14.77 ± 1.77	Ocak et al. [26]
SCN-0.16 DC	SCN-13.9 DC	311.50		0.34		5.39 ± 0.27	7.88 ± 0.79	14.95 ± 1.79	Keşlioğlu et al. [27]
SCN	SCN-9.55 NPG	317.10		0.34		5.43 ± 0.50	8.09 ± 1.21	14.22 ± 2.28	Karadağ et al. [51]
SCN	SCN-0.5 DIB	328		0.33		5.46 ± 0.55	8.25 ± 1.24	15.84 ± 2.53	[PW]

that this agreement for nonmetallic materials is due to the low melting point of organic materials.

The grain boundary energy

The grain boundary energy (σ_{gb}) can be expressed by [17–19]

$$\sigma_{gb} = 2\,\sigma_{SL}\cos\theta \tag{9}$$

where $\theta = \frac{\theta_A+\theta_B}{2}$ is the angle that the solid–liquid interface make with the y axis. The values of θ_A and θ_B were obtained from the cusp coordinates (x, y) using a Taylor expansion for parts at the base of the groove. The mean value of the grain boundary energy was then calculated by Eq. (9) using the mean value of the solid–liquid interfacial energy and the values of θ. The estimated error in the determination of angles was found to be 1 % from the standard deviation. Thus, the total experimental error in the resulting grain boundary energy is about 16 %. The mean value of grain boundary energy (σ_{gb}) for solid SCN in equilibrium with SCN-0.5 mol% DIB eutectic liquid was found to be $(15.84 \pm 2.53) \times 10^{-3}$ J m^{-2}.

Conclusions

Experiments were performed to directly observe the grain boundary groove shapes for equilibrated solid SCN in equilibrium with the SCN–DIB liquid. A thin liquid layer was melted, and the specimen was annealed in a constant linear temperature gradient for enough time to observe the equilibrated grain boundary groove shapes. The ratio of thermal conductivity of the equilibrated SCN-0.5 mol% DIB eutectic liquid to thermal conductivity of solid SCN was determined with a Bridgman-type growth apparatus. The Gibbs–Thomson coefficient, the solid–liquid interfacial energy and the grain boundary energy of solid SCN in equilibrium with the SCN-0.5 mol% DIB liquid have been determined from the observed grain boundary groove shapes.

Acknowledgements This project was supported by Erciyes University Scientific Research Project Unit under Contract No: FYL-2013-4628. The authors are grateful to Erciyes University Scientific Research Project Unit for their financial supports.

References

1. Eustathopoulos N, Nicholas MG, Drevet B. Wettability at High temperatures (Pergamon Materials Series). Oxford: Pergamon; 1999.
2. Martin JW, Doherty RD, Cantor B. Stability of microstructure in metallic systems (Cambridge Solid State Science Series). Cambridge: Cambridge University Press; 1997.
3. Turnbull D. Formation of crystal nuclei in liquid metals. J Appl Phys. 1950;2:1022.
4. Jones DRH. The free energies of solid–liquid interfaces. J Mater Sci. 1974;9:1.
5. Eustathopoulos N. Energetic of solid–liquid interfaces metals and systems. Int Met Rev. 1983;28:189.
6. Bolling GF, Tiller WA. Growth from the melt. I. Influence of surface intersection in pure metals. J Appl Phys. 1960;31:1345.
7. Jones DRH, Chadwick GA. Experimental measurement of solid–liquid interfacial energies of transparent materials. Philos Mag. 1970;22:291.
8. Nash GE, Glicksman ME. A general method for determining solid–liquid interfacial free energies. Philos Mag. 1971;24:577.
9. Jones DRH. Philos Mag. 1972;20:569.
10. Hardy SC. A grain boundary groove measurement of the surface tension between ice and water. Philos Mag. 1977;35:471.
11. Singh NB, Glicksman ME. Determination of the mean solid–liquid interface energy of pivalic acid. J Cryst Growth. 1989;98:573.
12. Garanasy L, Tegze M, Ludwig A. Solid–liquid interfacial free energy. Mater Sci Eng A Struct Prop. 1991;133:577.
13. Ketcham WM, Hobbs PV. Experimental determination of the surface energies of ice. Philos Mag. 1969;19:1161.
14. Thomas JD, Staveley AK. Study of the supercooling of droplets of some molecular liquids. J Chem Soc. 1952;45:69.
15. Hoyt JJ, Asta M, Haxhimali T, Karma A, Napolitano RE, Trivedi R, Laird BB, Morris JR. Crystal–melt interfaces and solidification morphologies in metals and systems. MRS Bull. 2004;29:935.
16. Trivedi R, Hunt JD. The mechanics of solder system wetting and spreading. New York: Van Nostrand Reinhold; 1993. p. 191.
17. Gündüz M, Hunt JD. The measurement of solid–liquid surface energies in the Al–Cu, Al–Si Pb–Sn systems. Acta Metall. 1985;33:1651.
18. Gündüz M, Hunt JD. Solid–liquid surface energies in the Al–Mg systems. Acta Mater. 1989;37:1839.
19. Maraşlı N, Hunt JD. Solid–liquid surface energies in the Al–$CuAl_2$, Al–$NiAl_3$ and Al–Ti systems. Acta Mater. 1996;44:1085.
20. Bayender B, Maraşlı N, Çadırlı E, Şişman H, Gündüz M. Solid–liquid surface energy of pivalic acid. J Cryst Growth. 1998;194:119.
21. Bayender B, Maraşlı N, Çadırlı E, Gündüz M. Solid–liquid surface energy of campene. Mater Sci Eng A Struct Prop. 1999;270:343.
22. Hunt JD, Jackson KA, Brown H. Temperature-gradient microscope stage suitable for freezing materials with melting points between −100 and 200 degrees. Rev Sci Instr. 1966;37:805.
23. Maraşlı N, Keşlioğlu K, Arslan B. Solid–liquid interface energies in the succinonitrile and succinonitrile–carbon tetrabromide system. J Cryst Growth. 2003;247:613.
24. Böyük U, Maraşlı N. Investigation of liquid composition effect on Gibbs–Thomson coefficient and solid–liquid interfacial energy in SCN based binary systems. Mater Charact. 2008;59:998.
25. Böyük U, Keşlioğlu K, Erol M, Maraşlı N. Measurement of solid–liquid interfacial energy in succinonitrile–pyrene system. Mater Lett. 2005;59:2953.
26. Ocak Y, Akbulut S, Böyük U, Erol M, Keşlioğlu K, Maraşlı N. Solid–liquid interfacial energy for solid succinonitrile in equilibrium with succinonitrile dichlorobenzene liquid. Thermochim Acta. 2006;445:86.
27. Keşlioğlu K, Böyük U, Erol M, Maraşlı N. Experimental determination of solid–liquid interfacial energy for succinonitrile solid solution in equilibrium with the succinonitrile–(D) camphor liquid. J Mater Sci. 2006;41:7939.
28. Akbulut S, Ocak Y, Böyük U, Erol M, Keslioğlu K, Maraşlı N. Measurement of solid -liquid interfacial energy in the pyrene succinonitrile monotectic system. J Phys Condens Matter. 2006;18:8403.

29. Ocak Y, Akbulut S, Böyük U, Erol M, Keşlioğlu K, Maraşlı N. Measurement of solid–liquid interfacial energy for solid D-camphor solution in equilibrium with succinonitrile D-camphor liquid. Scr Mater. 2006;55:235.
30. Pehlivanoğlu T, Böyük U, Keşlioğlu K, Ülgen A, Maraşlı N. Interfacial energies of p-dichlorobenzene succinonitrile system. Thermochim Acta. 2007;463:44.
31. Kant S, Reddi RSB, Rai RN. Solid–liquid equilibrium, thermal, crystallization and microstructural studies of organic monotectic alloy. Fluid Phase Equilib. 2010;291:71–5.
32. Gruggel RN, Well AG. Alloy solidification in systems containing a liquid miscibility gap. Metall Trans A. 1981;12:669–81.
33. Herlach DM, Cochrane RF, Egry I, Fecht HJ, Greer AL. Containerless processing in the study of metallic melts and their solidification. Int Mater Rev. 1993;38:273.
34. Trivedi R, Kurz W. Dendritic growth. Int Mater Rev. 1994;32:49–74.
35. Majumdar B, Chattopadhyay K. Metall Trans A. 1996;27:2053–7.
36. Glicksman ME, Singh NB, Chopra M. Gravitational effects in dendritic growth. Manuf Space. 1982;11:207–18.
37. Rai US, Rai RN. Some physicochemical studies on organic eutectics and molecular complex: urea–p-nitrophenol system. J Mater Res. 1999;14:1299–305.
38. Teng J, Liu S. Re-determination of succinonitrile (SCN)–camphor phase diagram. J Cryst Growth. 2006;290:248–57.
39. Farges JP. Organic conductors. New York: Marcel Dekker Inc.; 1994.
40. Gunter P. Nonlinear optical effects and materials. Berlin: Springer; 2000.
41. Singh NB, Henningsen T, Hopkins RH, Mazelsky R, Hamacher RD, Supertzi EP, Hopkins FK, Zelmon DE, Singh OP. Nonlinear optical characteristics of binary organic system. J Cryst Growth. 1993;128:976–80.
42. Derby B, Favier JJ. A criterion for the determination of monotectic structure. Acta Metall. 1983;7:1123–130.
43. Ecker A, Frazier DO, Alexander JID. Fluid flow in the melt of solidifying monotectic alloys. Metall Trans A. 1989;20:2517–27.
44. Alarco PJ, Yaser AL, Abouimran A, Armand M. The plastic-crystalline phase of succinonitrile as a universal matrix for solid-state ionic conductors. Nate Mater. 2004;3:476–81.
45. http://www.omkarchemicals.com/diiodobenzene.html.
46. Porter DA, Easterling KE. Phase transformations in metals and systems. UK: Van Nostrnad Reinhold Co., Ltd.; 1991.
47. McCartney DG, D Phil Thesis: University of Oxford: UK; 1981, p. 85.
48. Derollez P, Lefebvre J, Descamps M, Press W, Fontaine H. Structure of succinonitrile in its plastic phase. Condens Mater. 1990;2:6893–903.
49. Jones H. An evaluation of measurements of solid/liquid interfacial energies in metallic system systems by the groove profile method. Metall Mater Trans A. 2007;38A:1563.
50. Schaefer RJ, Glicksman ME, Ayers JD. High-confidence measurement of solid/liquid surface energy in a pure material. Philos Mag. 1975;32:725–43.
51. Karadağ SB, Altıntas Y, Öztürk E, Aksöz S, Keşlioğlu K, Maraşlı N. Solid–liquid interfacial energy of solid succinonitrile solution in equilibrium with succinonitrile–neopentylglycol eutectic liquid. J Cryst Growth. 2013;380:209–17.